

Enhanced deposition to pits: A local food source for benthos

by Patricia L. Yager¹, Arthur R. M. Nowell¹ and Peter A. Jumars¹

ABSTRACT

Particle deposition experiments using mimics of biogenous negative relief (“pits”) and low-excess-density particles in a small annular flume indicate a significantly enhanced deposition rate (number of particles per time) compared to smooth, flat patches of the same diameter. This study included flow visualizations as well as observations of particle residence times, particle concentrations in the pits, and particle fluxes to the pits from the main flow. Experimental conditions of particle concentration, shear velocity, and particle settling velocity mimicked the dynamic characteristics (low excess density and large size) of organic-rich flocs and flow conditions in the subtidal and deep sea where biogenous pits are common features. Results suggest that pits provide benthic organisms an important capture mechanism for such flocs. Flow visualizations concur qualitatively with previously reported results for two-dimensional cavity flow, with unique features due to the conical shape of the pits. When the Rouse number (settling velocity/shear velocity) was much less than 1, pit deposition rate increased with increasing pit aspect ratio ($AR = \text{depth/diameter}$; ranging from 0.25 to 2) and always exceeded deposition to a flat patch of comparable diameter. For the single aspect ratio tested ($AR = 0.5$) under conditions of increasing turbulence, deposition to the pit increased under transitional flow, but then decreased to near zero when conditions reached fully rough flow. Relative enhancement of deposition to this pit decreased with increased ambient bed roughness since gravel beds also effectively collect particles. Particle concentration inside pits decreased weakly with pit aspect ratio but greatly increased with increasing roughness Reynolds number. Particle residence time increased somewhat with pit aspect ratio but decreased significantly with increasing roughness Reynolds number. Particle flux into pits from the main flow increased with both increasing aspect ratio and increasing roughness Reynolds number. Enhancement of food supply to pit inhabitants thus depends on the flow regime.

1. Introduction

The sea floor rarely is smooth. Biogenous traces, tracks, mounds, tubes, and pits, as well as geological roughness, dominate the landscape of the ocean bottom (Heezen and Hollister, 1971). These features strongly affect small-scale fluid motions near the boundary and, consequently, local rates of deposition and erosion (Nowell and Jumars, 1984; Self *et al.*, 1989). Perturbations due to microtopography

1. School of Oceanography, WB-10, University of Washington, Seattle, Washington, 98195, U.S.A.

can thus significantly influence the food supply of both deposit- and suspension-feeding benthic organisms.

Depressions in aquatic sediments frequently are generated by some type of feeding behavior. Pits of many different sizes are formed by marine mammal suction feeding (Nelson *et al.*, 1987), epibenthic fish feeding or resting (Cook, 1971; Howard and Dörjes, 1972; Howard *et al.*, 1977; Risk and Craig, 1976; VanBlaricom 1982), funnel-producing, subsurface deposit feeding (Howard and Dörjes, 1972; Myers, 1977a,b), pit-dwelling surface deposit feeding (Nowell *et al.*, 1984), and pit-dwelling suspension feeding (Soluk and Craig, 1988). While it is not clear that pit-building or pit-dwelling costs an organism significant energy (see for example the Taghon, 1988, analysis for deposit feeders in which the mechanical costs of feeding are negligible), we predict using optimal foraging theory and the principle of lost opportunity (Stephens and Krebs, 1986; Jumars *et al.*, 1990) that pit dwellers receive some benefit from their lifestyle. In addition, if pit morphology and the ambient flow field influence these benefits, we predict that an organism will build a better pit under a given flow field.

Under some field conditions, pits, like ripple troughs, tend to fill in with finer-than-background sediments (Nelson *et al.*, 1987; Risk and Craig, 1976). In the deep sea, depressions are also known as sites for selective deposition of phytodetritus (Aller and Aller, 1986; Thiel *et al.*, 1988). The possibility for enhanced or selective deposition into pits elicits questions about food supply for benthic deposit feeders and suspension feeders and about passive meiofaunal and larval recruitment. Since pits are often associated with feeding behaviors, a primary interest is the effect that a pit has on its producer's or inhabitant's food supply, specifically the rate of supply of high-quality food due to an enhanced local deposition rate of low-excess-density, organic material (Jumars *et al.*, 1990). Another primary interest is the effect on larval recruitment (Thistle, 1981; VanBlaricom 1982). Both processes entail deposition of large, low-excess-density particles. This study investigates the hypothesis that pits function as preferred-particle collection devices for benthic organisms.

If pits can function to collect high-quality food particles, what determines their effectiveness? Field observations suggest a coupling of pits with environmental setting. We have observed a variety of pit shapes and aspect ratios in the field. In general, we have found that broad, shallow pits tend to be found in lower-energy environments, and narrow, steep-sided pits in higher-energy environments (personal observations by the authors). Pits are usually rare or absent in areas with either very low or very high energy (e.g. Yingst and Aller, 1982). These observations suggest strong feedback between feeding strategy, flow, and sediment transport regime.

Numerical models and flow visualization experiments of shear-layer driven cavity flow (Brandeis, 1982; O'Brien, 1972; Sinha *et al.*, 1982; Takematsu, 1966; Taneda, 1979; Weiss and Florsheim, 1965) suggest that the key parameters determining the

flow field of a pit are aspect ratio ($AR = H/D$, where H is pit depth and D is pit opening diameter) and pit Reynolds number ($Re = UL/\nu$, where U is mean flow velocity or the horizontal flow velocity at the pit opening, L is a pertinent length scale of the pit geometry, such as pit depth or diameter, and ν is the kinematic viscosity of the fluid). Analyses of sediment-trap collection support this parameterization, with important additional parameters including particle characteristics such as effective particle Rouse number ($w_p/\kappa u_*$, where w_p is the settling velocity of the particle, κ is von Karman's constant, ~ 0.41 , and u_* is the shear velocity of the flow), particle excess density ($\rho_p - \rho_f$, where ρ_p is the density of the particle and ρ_f is the density of the fluid), and volumetric particle concentration (fraction of total volume made up by particles) (Gardner, 1980a,b; Butman, 1986; Butman *et al.*, 1986). A true dimensional analysis for this class of flows has been done only for sediment traps (Butman *et al.*, 1986). The system we studied combines aspects from both cavity flow and the sediment-trap flow system. As such, it required its own treatment in order to address the question of whether benthic pits could function as traps for organic-rich particles.

To determine important dimensionless parameters that might be unique to the pit deposition system, we used a dimensional analysis method like that of Butman *et al.* (1986) to parameterize a pit trapping rate (P = number of particles trapped by the pit per unit time) as a function of 10 independent variables (see also Isaacson and Isaacson, 1975, for a complete description of this method). These variables and their basic dimensions (M = mass, L = length, T = time) are listed below:

1. D = pit diameter (L),
2. H = pit depth (L)
3. d = particle diameter (L)
4. ρ_p = particle density (ML^{-3})
5. ρ_f = fluid density (ML^{-3})
6. μ_f = fluid dynamic viscosity ($ML^{-1}T^{-1}$)
7. u_* = fluid shear velocity (LT^{-1})
8. k_s = bed roughness (L)
9. g = gravitational acceleration (LT^{-2})
10. N_c = number of particles in the fluid per unit volume (L^{-3})

Ten independent variables with three basic dimensions yield a minimum of seven dimensionless parameters. Our results resemble those of Butman *et al.* (1986) except for our addition of a roughness Reynolds number to characterize the boundary layer

flow. The resulting seven, physically relevant dimensionless parameters include:

- Π_1) dimensionless particle excess density ($S - 1$, where $S = \rho_p/\rho_f$),
- Π_2) particle Reynold's number ($w_p d/\nu$, where particle settling velocity, $w_p = (S - 1)gd^2/\nu$, and $\nu = \mu_f/\rho_f$),
- Π_3) volumetric concentration ($N_c d^3$, or more appropriately for spherical particles, $N_c 4\pi(d/2)^3/3$; or v_p/v_f where v_p is particle volume per fluid volume, v_f),
- Π_4) particle Rouse number (w_p/u_* , or more commonly, $w_p/\kappa u_*$, where κ is von Karman's constant = 0.41),
- Π_5) pit Reynolds number ($u_* D/\nu$),
- Π_6) pit aspect ratio (H/D ; for cone-shaped pits, this could also be expressed as slope angle for the pit side wall, $\phi = 90 - \tan^{-1}(D/2H)$), and
- Π_7) flow roughness Reynolds number ($u_* k_s/\nu$).

Our experimental design kept Π_1 – Π_3 constant during all experiments at conditions with dynamic similarity to chosen field conditions (Table 1). Across realistic ranges in values (Table 1), we varied either Π_6 (when we studied different pit geometries under smooth turbulent flow), or Π_4 , Π_5 , and Π_7 (when we studied the effect of flow turbulence on a single pit aspect ratio).

Our choice to mimic deep-sea aggregates with low-excess-density particles having large diameters reflects personal observations of deep-sea particles (Jumars *et al.*, 1990) and by the relatively few but critical, quantitative but non-destructive measurements of marine snow characteristics (e.g. Alldredge and Gotschalk, 1988). Since they have such low excess densities, and thus low settling velocities, such particles will generally remain in suspension or be easily eroded if ever deposited. These particles should rarely travel as bedload since their Rouse number is most often below 1 (see for example discussions in Middleton and Southard, 1985). Thus, they are most commonly accessible to suspension-feeding benthos only. If pits can effectively trap these particles from suspension, they can enhance the food supply to benthic deposit feeders. L. Mayer *et al.* (in review) finds such particles to be far higher in labile organic material than are bulk sediments. Pits, therefore, could dramatically improve the diet of their deposit-feeding inhabitants.

Our experimental study shows how pits significantly alter the local fluid and depositional environment, infers how they affect depositional mechanisms for organic flocs, and begins to resolve the possible feedback between pit aspect ratio and the surrounding flow field. These ideas remain untested in the field as does the particle selectivity that pits may offer to their inhabitants.

2. Methods

Two different types of experiments used two different flumes. In any experiment, the choice of flume requires some compromise (see Nowell and Jumars, 1987). For

flow visualization in and around the pits, we used a straight, non-recirculating flume that permits the use of fluorescent dye, although maximum attainable velocity was relatively low compared to common field conditions and surface waves at the air-water interface complicated quantitative measurements. For deposition experiments, we used an annular recirculating flume that maintains a nearly constant concentration of particles in a flow field without surface waves, but has a narrow channel and significant ($\sim 10\%$ of downstream) cross-stream circulation. While these compromises should not strongly influence the overall results of our experiment, they should be kept in mind when comparing our measurements to those of others or to the field.

Four pit mimics were lathed from solid PVC into conical shapes. Pits had opening diameters (D) of 3.0 cm and depths (H) of 0.75, 1.5, 3.0, and 6.0 cm, leading to aspect ratios ($AR = H/D$) of 0.25, 0.5, 1.0, and 2.0, and wall angles, ϕ , of 26.6, 45.0, 63.4 and 75.5°, respectively. All but the shallowest pit, then, exceed the mass angle of repose ($\phi_r \sim 35^\circ$) held by non-cohesive sediments (Smith and Lohnes, 1984) and thus mimic conditions with cohesive sediments or biological adhesives. Pits were machined to fit with their openings flush with the bottoms of the flumes.

Using fluorescent dye, we determined the basic flow structure in and around all the pits with observations and photographs in the straight, non-recirculating flume (described by Eckman *et al.*, 1981) at relatively low flow velocities ($u_z = 1$ and 4 cm s^{-1} at $z = 10 \text{ cm}$, $u_* = 0.07$ and 0.2 cm s^{-1} , and $h = 10 \text{ cm}$, where u_z is the downstream velocity at z , the height above bottom, u_* is the shear velocity, and h is water depth). For the deposition experiments, in an annular flume first described by Taghon *et al.* (1984) and subsequently modified and used by Miller (1989), we tested the effect of pit aspect ratio (AR) and near-bed turbulence levels (expressed as roughness Reynolds number, $Re_* = u_* k_s / \nu$, where k_s is the roughness length scale of the bed) on particle deposition into the pit and onto a flat patch of the same diameter. Pit aspect ratios and fluid velocities were chosen to represent subtidal or deep-sea environments (see Table 1). Steady velocities were driven and maintained at 10 or 20 cm s^{-1} ($\pm 0.3 \text{ cm s}^{-1}$) by a shear plate on the water surface, 10 cm above the bed, controlled by a central, variable-speed motor driving a cross-beam (Miller, 1989). The bed of the flume was either smooth acrylic (for the hydraulically smooth condition; $k_s \leq 0.01 \text{ cm}$) or a 2-cm thick layer of pea gravel (to achieve transitional and rough flow conditions; $k_s = 1 \text{ cm}$). Shear velocities (u_*), approximated from shear-plate velocities and assuming a logarithmic velocity profile were 0.5 and 0.9 cm s^{-1} for the smooth-bed treatments with low and high velocity, respectively, and 0.7 and 1.4 cm s^{-1} for gravel-bed treatments with low and high velocity, respectively. Roughness Reynolds numbers (Re_*) were calculated to be 0.4 and 0.8 (hydraulically smooth; $Re_* \leq 1$), 60 (transitional), and 120 (fully rough; $Re_* \geq 100$). Cross-stream flow within the annular flume (about 10% of the downstream flow) makes these values approximate.

Table 1. Dimensionless parameters: dynamic similarity between experiment and field values.

Dimensionless parameter	Value in this study	Value for subtidal/deep sea	Citations for field values
Π_1 : particle excess density ($S = \rho_p/\rho_s$)	$S = 1.001$ ($S - 1$) = 9.6×10^{-4}	$S = 1.02$ to 1.00 ($S - 1$) = 2.2×10^{-2} to 1.3×10^{-5}	Alldredge & Gotschalk (1988) ¹
Π_2 : particle Reynolds number ($Re_p = w_p d/\nu$)	0.14 ± 0.064	Marine snow: 0.2 to 7.0 0.305 to 0.98 Polychaete larvae: 0.04 to 2.3	Alldredge & Gotschalk (1988) ² McCave (1984a) ³ Hannan (1984) ⁴
Π_3 : volumetric concentration (V_p/V_f)	0.0013^5	—	—
Π_4 : particle Rouse number ($w_p/\kappa u_*$)	HSF ⁶ : 0.11 ± 0.030 HSF: 0.059 ± 0.017 HTF: 0.076 ± 0.022 HRF: 0.038 ± 0.011	0.03 to 1.6	Gross & Dade (1991) combined with Alldredge & Gotschalk (1988) ⁷
Π_5 : pit Reynolds number ($u_* D/\nu$)	HSF: 130 HSF: 230 HTF: 180 HRF: 360	15 to 2500	Mauviel <i>et al.</i> (1987), Billheimer and Coull (1988), Palmer (1988) combined with Gross & Dade (1991) ⁸
Π_6 : pit aspect ratio (H/D)	HSF: $0.25, 0.5, 1, 2$ HTF: 0.5 HRF: 0.5	Ichnofossils: 0.13 to 5.0 Modern: 0.4 to 0.6	Pemberton <i>et al.</i> (1988) Mauviel <i>et al.</i> (1987), Billheimer and Coull (1988), Palmer (1988)

Table 1. (Continued)

Dimensionless parameter	Value in this study	Value for subtidal/deep sea	Citations for field values
wall angle ($\phi = 90 - \tan^{-1}(D/2H)$)	$\{\phi_r = 27, 45, 63, 76\}$	$\phi_r \sim 35^\circ$; non-cohesive quartz	Smith and Lohnes (1984)
Π_7) flow roughness Reynolds number ($u_* k_s / \nu$)	HSF: 0.4 HSF: 0.6 HTF: 60 HSF: 120	3 to 150	Gross & Dade (1991) combined with Wheatcroft (1990) ⁹

¹The range measured by divers in surface waters off Southern California. From their regression equation, $\Delta\rho = (1.8 \times 10^{-3})$ (diameter, in mm)^{-1.6} and $\rho_f = 1.02488$, a 700 μm particle has $S = 1.003$ or $S - 1 = 3.11 \times 10^{-3}$. See also Jumars et al., 1990, for a qualitative description of the “tumbleweed-like” nature of deep-sea aggregates.

²Range for all particles measured (diameters from 0.5 to 25.5 mm). Using their regression for settling velocity, w_p (m day⁻¹) = 50 (diameter; in mm)^{0.26}, the Reynolds number for a 700 μm particle is about 0.3.

³Range reported for model parameters with particle size range from 500 to 1000 μm .

⁴Computed using w_n values from Table 3.6, larval length, and $\nu = 0.01 \text{ cm}^2 \text{ s}^{-2}$.

⁵Chosen to be high enough to expedite experimental method while still being below a concentration which would have initiated hindered settling (5–10 kg m⁻³, McCave, 1984b). While relative concentration is important in terms of the overall efficiency of pit capture, it is not a dynamic property.

⁶Where HSF is hydraulically smooth flow ($Re_* < 1$), HTF is hydraulically transitional flow, and HRF is hydraulically rough flow ($Re_* \geq 100$).

⁷Computed from the u_* range reported for the HEBBLE site: 0.3 to 1.5 cm s⁻¹, the settling velocity range reported for shallow-water marine snow (no one has measured deep-sea marine snow without using pumps): 0.02 to 0.2 cm s⁻¹, and von Karman’s constant, $\kappa = 0.41$.

⁸Computed from the u_* range reported for the HEBBLE site (0.3 to 1.5 cm s⁻¹; Gross and Dade, 1991) and a range of values found in the literature for opening diameters of pits (0.3 to 15 cm), $\nu = 0.01$.

⁹Computed using HEBBLE-site u_* (0.3 to 1.5 cm s⁻¹; Gross and Dade, 1991) and deep-sea roughness length scales, k_s , of 0.1 to 1.0 cm (Wheatcroft, 1990), $\nu = 0.01 \text{ cm}^2 \text{ sec}^{-2}$.

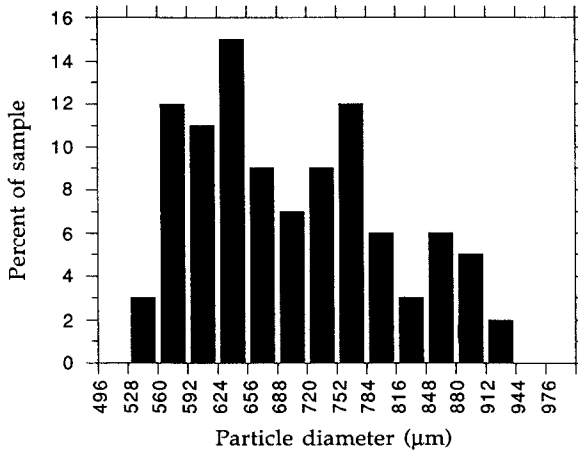


Figure 1. Size frequency distribution of the polystyrene latex spheres, based on microscopic measurements of 100 particles. Mean diameter is 0.070 cm; median diameter is 0.067 cm.

Polystyrene latex spheres (mean diameter, ± 1 s.d., equals $704 \pm 102 \mu\text{m}$, see Fig. 1; $\rho_p = 1.046 \text{ g cm}^{-3}$) in filtered, hypersaline flume water ($\rho_f = 1.045 \text{ g ml}^{-1}$, $\nu = 0.0116 \text{ cm}^2 \text{ s}^{-1}$) were used to mimic organic flocs with large diameters and low excess densities (see Table 1). Particle concentration was held constant at 0.13% by volume (or 7 ± 4 beads ml^{-1} given the volumes of spherical beads with the above grain-size distribution). A small amount of Triton-X-100[™] (polyoxyethelene ether, Union Carbide Chemicals and Plastics Co., Inc.) dispersant was added to the bead slurry to prevent the hydrophobic beads from clumping and ease their introduction to the flume water. This detergent prevents aggregation of the particles, but had no effect on whether particles deposit. Particles were introduced slowly and consistently to the already-running flume via a funnel at a point source on the opposite side of the flume from the pit (time elapsed about 2 min). Over the 20-min time course of the experiment, particle concentration remained essentially uniform throughout the flume, with minor losses of particles to an inner zone of lower shear. Temperature ($\pm 0.5^\circ\text{C}$) and density ($\pm 0.0005 \text{ g ml}^{-1}$; measured using a hydrometer) of the flume water were carefully monitored before and after each run since our results were very sensitive to particle excess density (data not shown).

Pits were installed flush with the bottom at a single site in the flume (only one *AR* per run). Patches were drawn centered on the flume bottom (or distinguished by white gravel) to have diameters equal to that of the pit opening (3 cm). The one pit and three patch locations were distributed 90° apart around the circular flume. The average number of particles depositing to the three patches was used for comparison to the pit, although the results did not depend significantly on the patch or patches chosen. Pit walls and smooth patches were coated thinly and uniformly with an adhesive wax (Swix[™] cross-country ski wax, “wet snow” formula) so that deposition

rate was equal to encounter rate (i.e., the post-contact sticking efficiency was 100%, and there was no re-entrainment under any flow conditions tested; this assertion was confirmed by close inspection of the pits using video). Gravel patches received no adhesive. Consequently, for the gravel-bed cases, we measured both “gross” and “net” patch deposition, using video to count every particle that landed on and disappeared into the gravel (“gross”), as well as those that were subsequently re-entrained (the difference being “net” deposition). Since sticky pits had no particle re-entrainment, gross deposition to the patch (the total number of beads depositing on the patch) was used for all comparisons in lieu of making the gravel sticky. Relative to the flume volume and its stock of particles in suspension, the loss of particles from suspension to sticky pit walls was negligible.

Each pit AR treatment was repeated 6 times under one smooth flow condition. Each turbulence treatment (using only one of the pits, $AR = 0.5$) was repeated either 6 (smooth-bed treatments) or 3 times (gravel-bed treatments; the fewer number of runs is due to the time-intensive nature of their analyses). Ordering of runs was partly randomized in time, i.e. the ordering of AR treatments was random, but the runs for a single AR were done sequentially (to avoid inconsistent positioning of the pit on the flume bottom). Between each run, the entire flume setup was broken down, washed, and set up again with newly coated pit and patches, filtered flume water, and washed, remeasured particles. Video cameras equipped with Tameron 90 mm F/2.5 lenses were placed above each pit or patch, looking down from the top, to view their entire contents. Measurements were made by visual counts either during the experiment or on video tape from a Panasonic AG-6300 frame-by-frame video cassette recorder with a scanning frame rate of 30 Hz. For a single, randomly selected run from each treatment combination, we measured particle flux (the number of particles entering the pit per unit of time; determined by watching the video for ten separate, randomly-selected one-minute intervals and counting the number of particles to enter the pit), particle concentration (number of particles per unit of volume within the pit; determined by stopping the video randomly and counting the number of particles within the pit, repeated 30 times for each run), and residence time of particles within the pit (determined by following randomly-selected, individual particles during their time spent within the pit, repeated 13–30 times for each run). For all of these runs, we measured deposition rates to the pit and to the patches by counting the number of particles to deposit over the course of 20 min.

3. Statistical analysis

The Kolmogorov-Smirnov one-sample test for normality and Bartlett’s test for equality of variance (Sokal and Rohlf, 1981) were done first to determine whether parametric statistics could be used. Many of the data exhibited non-normal distributions and unequal variance. Further, the sample sizes were too small to assure us that

a transformation could be justified. These facts prevented the legitimate application of parametric tests. We therefore analyzed for treatment effects using nonparametric statistical tests. These tests are less powerful, but insensitive to non-normality. Because data are non-normally distributed, raw data are presented with lines connecting medians rather than means.

To test for differences among all treatments, we used the Kruskal-Wallis distribution-free test (*KW*; Hollander and Wolfe, 1973; Sokal and Rohlf, 1981). Standard tie corrections were made (Hollander and Wolfe, 1973). The conventional $\alpha = 0.05$ level was used as the criterion for significance of results. To test for significant differences between individual treatment pairs, we used an “unplanned” Mann-Whitney *U* or summed-ranks test (*MWU*; Sokal and Rohlf, 1981) and the conservative Bonferoni approximation of significance in multiple comparisons ($\alpha = 0.05/n$ where *n* is the number of unplanned multiple comparisons, Hollander and Wolfe, 1973). To determine whether variability across treatments signaled a linear trend, we used Theil’s nonparametric slope estimator (*TS*; Hollander and Wolfe, 1973). Kendall’s Rank Correlation Coefficient (τ ; Sokal and Rohlf, 1981) was used to determine the correlation between pit and patch results of a single run.

4. Results

a. Pit circulation

Flow patterns observed in the pits (Fig. 2) resemble those observed previously for two-dimensional, *V*-shaped cavities under Stokes flow (see Taneda, 1979, Fig. 19). Separation from the boundary occurs near the upstream edge of the pit. A dividing streamline (or streamplane) grows downward, ending at a stagnation point (or a stagnation line). Boundary-layer reattachment occurs near the downstream edge. Momentum transferred across the free-shear layer drives recirculation inside the pit. This general description holds for all pit aspect ratios tested here. Theory suggests that there are an increasing number of smaller and slower recirculating vortices continuing down into the apex of deeper ($AR > 1$) pits (Moffatt, 1964), each reversing direction as momentum is transferred from the base of the one above. The existence of these secondary vortices has been shown experimentally for two-dimensional, wedge-shaped cavities (Taneda, 1979) and some sediment traps (Gardner, 1980a). In our conical (three-dimensional) setup with fluorescent dye, we were unable to observe any lower vortices, perhaps because, as Taneda (1979) reported, they rotate three orders of magnitude more slowly than the uppermost vortex. Instead, the bottom of the deeper pits appeared to be “dead space” with a relatively long (up to several hours in the deeper pits) residence time.

Three-dimensional pit geometry under two-dimensional (horizontally-uniform) flow sets up a non-uniform pressure field that drives fluid exchange. Shear-driven

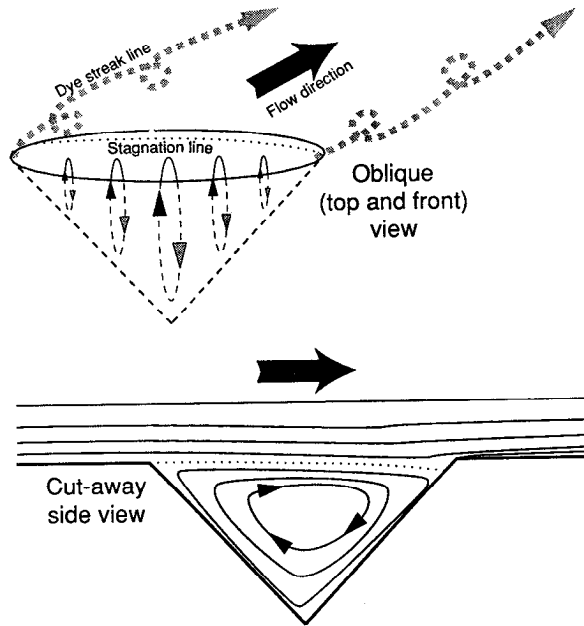


Figure 2. Qualitative patterns of flow observed in a conical pit ($AR = 0.5$) by following dye streaklines and particle paths. Bold arrows show predominant downstream flow direction. Generalized side view shows a single rotating vortex, growing wall boundary layers, and a stagnation streamline (dotted). Oblique view shows cross-stream gradient in vorticity resulting in the advection downstream of vortex filaments of dye initially injected into the pit. The shape of the vortices' is idealized, and the gray arrowheads show the rearward (downstream) sense of rotation.

rotation is faster on the shallower cross-stream edges than in the center of the pit. Since vorticity and angular momentum must be conserved, fluid from the center moves toward the sides and then exits as two vortex filaments advecting downstream (Fig. 2).

Fluid input to the pit was not steady but rather episodic when observed using dye. Only occasionally would a near-bed dye streak from upstream enter the pit. This fluid would most often but not exclusively enter along the downstream edge of the pit, similar to patterns observed with sediment traps (Butman, 1986; Gardner, 1980a). Fluid may enter the pit in the form of periodic sweeps through the free-shear layer or as periodic fluid injections arising from instabilities in the dividing streamline (or "streamplane"). These instabilities might be caused by fluid leaving the recirculation zone faster than it can enter, reducing volume under the streamplane. As the dividing streamplane is pulled downward it becomes unstable at some position, breaks away from the pit wall, allows fluid to enter the pit, and then reattaches where it is more stable.

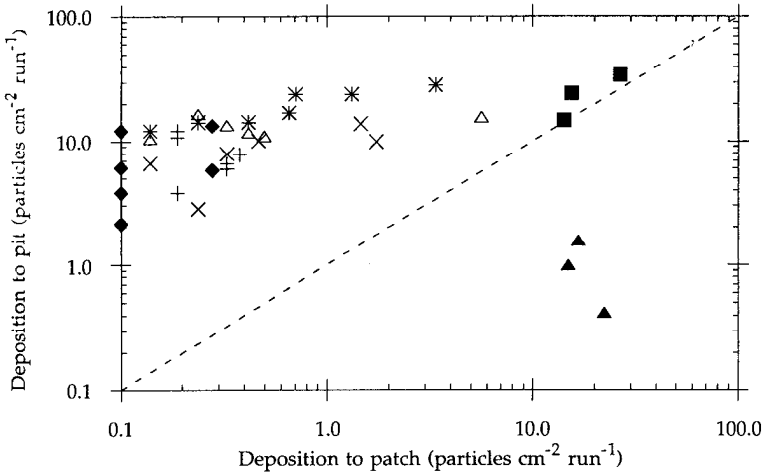


Figure 3. Deposition to pits (scaled by surface area of respective pit aspect ratio; particles $\text{cm}^{-2} \text{run}^{-1}$) as a function of patch deposition (particles $\text{cm}^{-2} \text{run}^{-1}$) for each experimental run (run = 20 min). For $Re_* = 0.4$: $AR = 1/4$ (+), $AR = 1/2$ (x), $AR = 1$ (Δ), $AR = 2$ (*). For $AR = 1/2$: $Re_* = 0.8$ (\blacklozenge), $Re_* = 60$ (\blacksquare), $Re_* = 120$ (\blacktriangle).] Dashed line indicates where data would fall if there were no enhancement by pits ($x = y$).

b. Pit deposition

Under hydraulically smooth conditions (smooth bed, $Re_* = 0.4$ or 0.8), all pit aspect ratios consistently captured more total particles than did patches. Under hydraulically transitional flow ($Re_* = 60$), the pit trapped slightly more or about the same as the highly efficient gravel bed. Only in the most turbulent, hydraulically rough case ($Re_* = 120$) did the pits no longer enhance particle deposition. These results hold even if pit capture is scaled to the additional surface area of the pit compared to the patch (Fig. 3).

i. Effects of Aspect Ratio. Particle flux significantly increased overall with increasing aspect ratio (Fig. 4A; *KW*, Table 2), but significant differences between pairs are found only between the deepest pit ($AR = 2$) and two ($AR = 0.25$ and 1) of the other three pit aspect ratios (*MWU*, Table 2). A significant linear relationship between particle flux and pit aspect ratio has a positive slope (*TS*, Table 2) from shallowest to deepest pits. Deviation from the linear relationship, while not statistically significant, appears to occur at pit AR of 0.5 for which the median flux increases somewhat.

Particle concentration in a pit decreased with increasing pit aspect ratio (Fig. 4B). Its range also decreased with increasing aspect ratio. Overall, a significant difference is seen among all the pit aspect ratios (*KW*, Table 2), but only the shallowest pit ($AR = 0.25$) differs significantly from each of the other three pit aspect ratios (*MWU*, Table 2). A significant linear ordering of treatments has a negative slope (*TS*, Table 2).

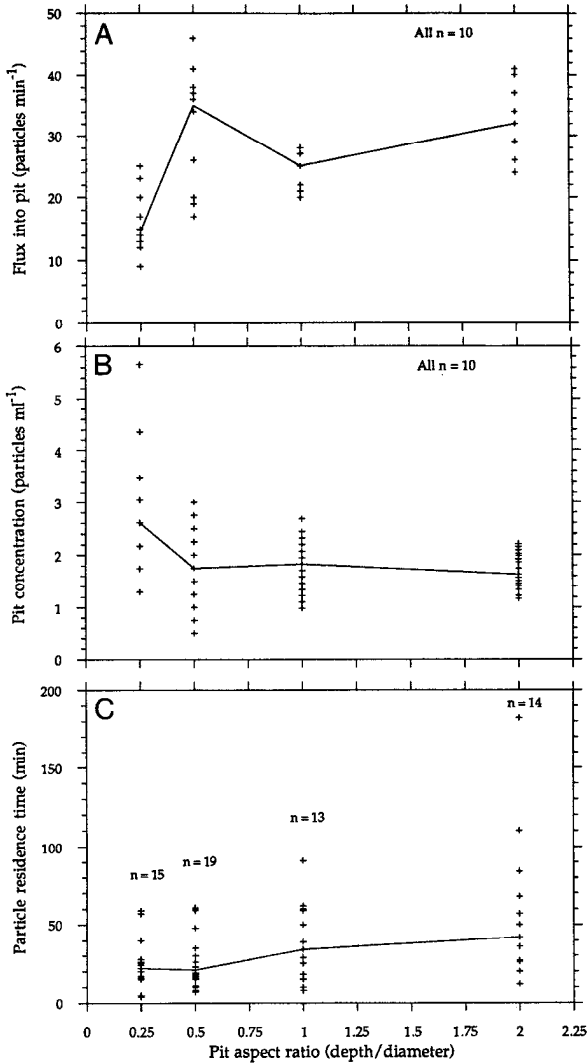


Figure 4. For $Re_* = 0.4$, particle transport into pits as a function of pit aspect ratio (pit depth/diameter): (a) particle flux into pit (particles min^{-1}); (b) particle concentration within pit (particles ml^{-1}); (c) particle residence time within pit (min). Median values for each distribution are connected by a line.

Particle residence time increased weakly with pit aspect ratio (Fig. 4C). Overall differences were found among pit aspect ratios (KW , Table 2) but the only significantly different pairs are the deepest and the two shallowest pits (MWU , Table 2). The distribution exhibits a weak but significant positive slope (TS , Table 2).

Deposition to the pit increased with increasing pit aspect ratio (Fig. 5A). An

Table 2. Statistical probabilities for comparisons of differences between pit aspect ratios ($Re_* = 0.4$).

Test	H_0	Treatment					
		Particle flux	Particle concentration	Residence time	Deposition to pit	Deposition to patch	Enhancement (pit/patch)
KRUSKAL-WALLIS:	$AR_{1/4} = AR_{1/2} = AR_1 = AR_2$	<u>$P = 0.006$</u>	<u>$P \leq 0.001$</u>	<u>$P = 0.036$</u>	<u>$P = 0.004$</u>	$P = 0.47$	$P = 0.45$
MANN-WHITNEY U:	$AR_{1/4} = AR_{1/2}$	$P \geq 0.10$	$P \leq 0.001$	$P \geq 0.10$	$P \geq 0.10$	$P \geq 0.10$	$P \geq 0.10$
	$AR_{1/4} = AR_1$	$P = 0.08$	<u>$P \leq 0.001$</u>	$P = 0.08$	$P = 0.025$	$P \geq 0.10$	$P \geq 0.10$
	$AR_{1/4} = AR_2$	<u>$P = 0.005$</u>	<u>$P \leq 0.001$</u>	<u>$P = 0.005$</u>	<u>$P \leq 0.005$</u>	$P \geq 0.10$	$P \geq 0.10$
	$AR_{1/2} = AR_1$	<u>$P \geq 0.10$</u>	$P = 0.61$	<u>$P \geq 0.10$</u>	<u>$P = 0.018$</u>	$P \geq 0.10$	$P \geq 0.10$
	$AR_{1/2} = AR_2$	$P = 0.02$	$P = 0.71$	<u>$P = 0.009$</u>	<u>$P = 0.005$</u>	$P \geq 0.10$	$P \geq 0.10$
	$AR_1 = AR_2$	<u>$P = 0.001$</u>	$P = 0.18$	<u>$P \geq 0.10$</u>	<u>$P = 0.05$</u>	<u>$P \geq 0.10$</u>	<u>$P \geq 0.10$</u>
THEIL SLOPE:	$\beta = 0$	<u>$P = 0.05$</u>	<u>$P = 0.001$</u>	<u>$P \leq 0.004$</u>	<u>$P \leq 0.001$</u>	<u>$P = 0.024$</u>	$P = 0.47$

Underlined values indicate significance at $\alpha = 0.05$ for Kruskal-Wallis and Theil slope or $\alpha = 0.05/n$ where $n = 6$ for Mann-Whitney U test.

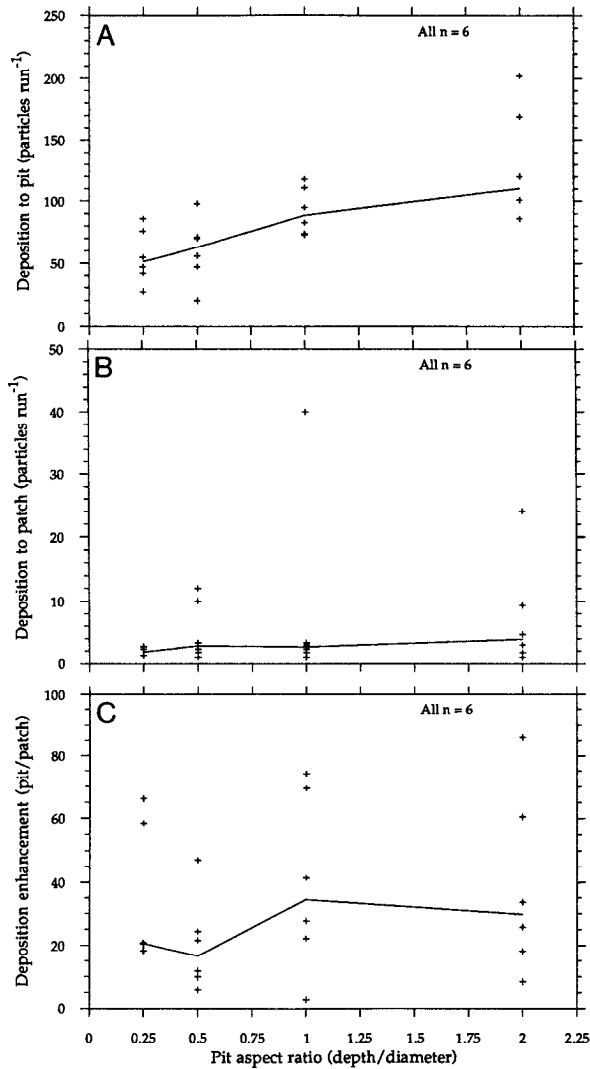


Figure 5. For $Re_* = 0.4$, particle deposition as a function of pit aspect ratio (pit depth/diameter) of each experimental run (run = 20 min): (a) particle deposition to pit (particles run⁻¹); (b) particle deposition to patch (particles run⁻¹); (c) particle deposition enhancement (particles into pit run⁻¹ scaled by particles onto patch run⁻¹). Median values for each distribution are connected by a line.

overall difference exists among pit aspect ratios (*KW*, Table 2). Significant differences occur between the deepest and the two shallowest pits (*MWU*, Table 2). A Theil regression gives a slope (β) of 42 with a 95% confidence interval from 22.3 to 66.3. If these data are scaled by dividing by the square root of internal pit surface area (one choice for a characteristic length scale), however, the differences among

them disappear ($KW; P \geq 0.50$), and the slope is not significantly different from zero ($TS; P = 0.15$). Scaling by whole surface area “overcompensates” for the trend and causes a negative slope. Thus, shallower pits are capturing more particles than is explained by their surface area (see also Fig. 3).

Patch deposition in each run was highly variable and not well correlated with pit deposition from the same run ($\tau; P = 0.09$; see Fig. 3). A slight trend existed in the patch data grouped according to pit treatment (Fig. 5B; $\beta = 0.95$, 95% confidence limits from -0.4 to 2.67), although differences among and between groups were not significant (KW, MWU , Table 2). A significant correlation would have implied that some uncontrolled variable varied systematically among runs.

Despite the lack of strong correlation between pit and patch deposition, to be conservative we present the data for deposition enhancement (pit deposition scaled by patch deposition) as it varies with pit aspect ratio (Fig. 5C). Once scaled, there are no significant overall or individual differences among or between aspect ratios (KW, MWU , Table 2) and no linear slope (TS , Table 2). Deposition enhancement by pits under hydraulically smooth flow is not a significant function of aspect ratio when determined in this manner over the range of aspect ratios used here. The large, unsystematic variation in patch deposition, however, appears responsible for this result, and a larger data set might show otherwise.

ii. Bed roughness and effects of turbulence. Particle flux into a pit ($AR = 0.5$) showed the strongest response of all our data to increasing turbulence (Fig. 6A). Under hydraulically smooth flow, particle flux did not change significantly with a doubling of surface velocity (MWU , Table 3). Yet, with the same surface velocity, adding gravel to the bed dramatically increased particle flux to the pit (MWU , Table 3). Under fully rough flow ($Re_* > 100$), particle flux increases significantly, compared to both smooth and transitional flow regimes (MWU , Table 3).

Particle concentration in the pit also increased dramatically with increasing turbulence intensity (Fig. 6B). An increase of velocity while still within hydraulically smooth flow did not affect concentration significantly (MWU , Table 3). Moving into flow regimes of greater turbulence, however, caused a significant increase in pit concentration (MWU , Table 3). In hydraulically rough flow, particle flux was increased more than enough to compensate for the shortened residence time and greater pit volume, and resulted in a very high number of beads in the pit.

Particle residence times showed no significant differences under hydraulically smooth and transitional flow conditions (Fig. 6C; MWU , Table 3). The change to hydraulically rough flow caused a marked decrease in particle residence time (MWU , Table 3). Overall, there was a significant decrease in residence time with increasing Re_* (KW , Table 3).

Deposition rates to the pit increased, then decreased as turbulence increased from smooth to transitional, then from transitional to rough flow (Fig. 7A). Pit deposition

Table 3. Statistical probabilities for comparisons of differences between Roughness Reynolds numbers ($AR = 0.5$).

Test	H_0	Treatment					
		Particle flux	Particle concentration	Residence time	Deposition to pit	Deposition to patch	Enhancement (pit/patch)
KRUSKAL-WALLIS:	$Re_{*0.4} = Re_{*0.8} =$	$P \leq 0.001$	$P \leq 0.001$	$P \leq 0.001$	$P < 0.01$	$P \leq 0.005$	$P \leq 0.005$
	$Re_{*60} = Re_{*120}$						
MANN-WHITNEY U:	$Re_{*0.4} = Re_{*0.8}$	$P = 0.10$	$P > 0.05$	$P \leq 0.05$	$P \geq 0.10$	$P = 0.04$	$P \leq 0.05$
	$Re_{*0.4} = Re_{*60}$	$P \leq 0.001$	$P \leq 0.001$	$P \leq 0.05$	$P \leq 0.01$	$P \leq 0.01$	$P \leq 0.01$
	$Re_{*0.4} = Re_{*120}$	$P \leq 0.001$	$P \leq 0.001$	$P \leq 0.001$	$P \leq 0.01$	$P \leq 0.01$	$P \leq 0.01$
	$Re_{*0.8} = Re_{*60}$	$P \leq 0.001$	$P \leq 0.001$	$P \geq 0.10$	$P \leq 0.01$	$P \leq 0.01$	$P \leq 0.01$
	$Re_{*0.8} = Re_{*120}$	$P \leq 0.001$	$P \leq 0.001$	$P \leq 0.001$	$P \leq 0.01$	$P \leq 0.01$	$P \leq 0.01$
	$Re_{*60} = Re_{*120}$	$P \leq 0.001$	$P \leq 0.001$	$P \leq 0.001$	$P \leq 0.05$	$P \geq 0.10$	$P \leq 0.05$

Underlined values indicate significance at $\alpha = 0.05$ for Kruskal-Wallis or $\alpha = 0.05/n$ where $n = 6$ for Mann-Whitney U test.

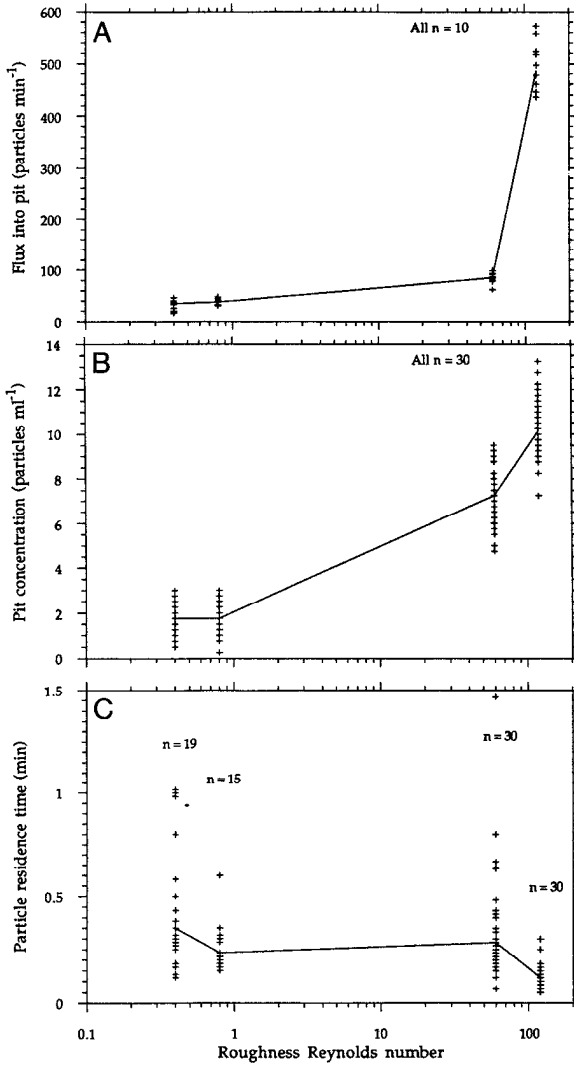


Figure 6. For $AR = 0.5$, particle transport into pits as a function of roughness Reynolds number ($Re_* = u_* k_s / \nu$): (a) particle flux into pit (particles min^{-1}); (b) particle concentration within pit (particles ml^{-1}); (c) particle residence time within pit (min). Median values for each distribution are connected by a line.

did not change significantly within smooth-bed cases (*MWU*, Table 3). Under transitional flow, pit deposition increased significantly (*MWU*, Table 3). Most depositional mechanisms, however, must shut down under hydraulically rough conditions since significantly fewer particles were captured in the pit (*MWU*, Table 3). Those particles that did deposit under rough conditions often did so at the pit

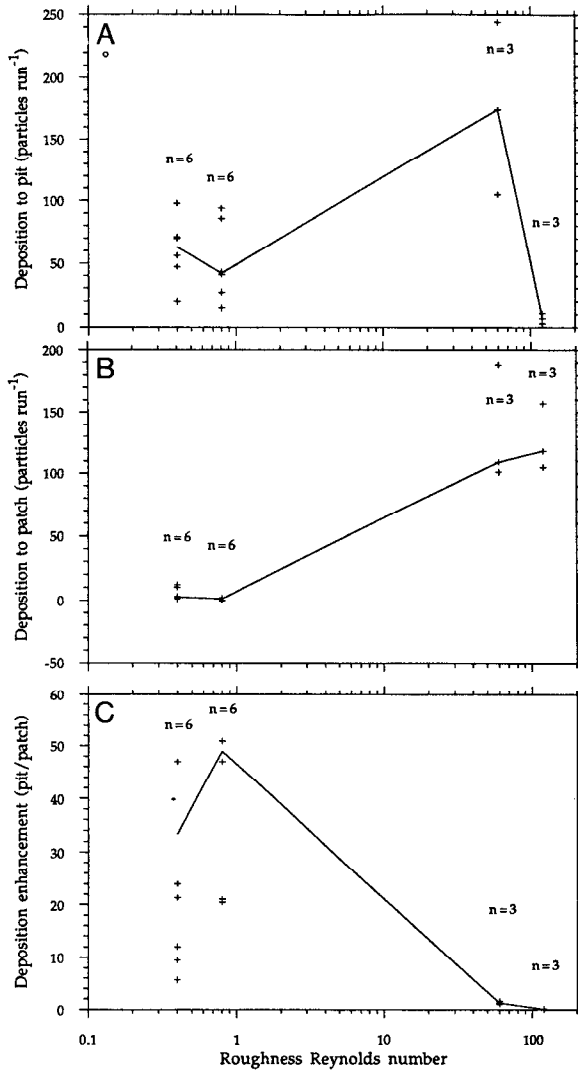


Figure 7. For $AR = 0.5$, particle deposition as a function of roughness Reynolds number ($Re_* = u_* k_s / \nu$) of each experimental run (run = 20 min): (a) particle deposition to pit (particles run⁻¹); (b) particle deposition to patch (particles run⁻¹); (c) particle deposition enhancement (particles into pit run⁻¹ scaled by particles onto patch run⁻¹). Median values for each distribution are connected by a line.

stagnation line. The decrease in deposition to the pit was not due to increased re-entrainment after deposition. Videotaped observations of individual particles showed no particle encounters with the adhesive-coated pit wall that did not result in permanent capture. Hence, under hydraulically rough flow, there were fewer encounters with the pit walls.

Patch deposition rates increased an order of magnitude with the addition of a gravel bed and enhanced near-bed turbulence (Fig. 7B). With a hydraulically smooth bed, deposition rates were low since few beads had any significant component of motion toward (rather than parallel to) the sticky surface. A change in bed roughness increased the number of particles deposited to the patch over time (Fig. 7B; *MWU*, Table 3) since particle motion near the bed had an increased vertical component and also since the beads could come to rest in the quiet spaces (or mini-pits) between gravel particles. Gross deposition rates to the gravel bed did not change significantly with increasing velocity or with the change from transitional to rough flow (*MWU*, Table 3). Net deposition, however, was significantly different and much lower for the more turbulent case since re-entrainment from the (non-adhesive-coated) gravel bed was much higher under fully rough flow (data not shown).

With a gravel bed, under hydraulically transitional flow, both the pit and the patch became efficient particle collectors (Fig. 7C). The enhancement ratio was just above one. With an increase in velocity, however, pits no longer collected many particles while the patches did. The enhancement ratio thus dropped below one, and the pits no longer acted as efficient particle collectors.

5. Discussion

Theoretical and experimental models support the concept that pit aspect ratio and the flow field together influence fluid and, consequently, the behavior of nearly-buoyant particles inside a pit. Under viscous flow (low Re), aspect ratio determines the shape and number of recirculating vortices in shear-plate-driven cavity flows (Bozeman and Dalton, 1973; Greenspan, 1969; Kawaguti, 1961; Mills, 1965b; Pan and Acrivos, 1967; Ratkowsky and Rotem, 1968; Takematsu, 1965; Torrance and Zien, 1972). Reynolds number determines the position of vortex centers and the intensity of vortex circulation (Burggraf, 1966; Greenspan, 1969; Kawaguti, 1961; Mills, 1965a; Nallasamy and Prasad, 1977; Pan and Acrivos, 1967). Models of shear-layer-driven cavity flows (Brandeis, 1982; O'Brien, 1972; Sinha *et al.*, 1982; Takematsu, 1966; Taneda, 1979; Weiss and Florsheim, 1965) further indicate that the shape of the dividing streamline and the intensity of circulation depend on cavity aspect ratio and the velocity profile over the cavity. Under viscous flow, shallower cavities ($AR \leq 1$) have lower circulation intensities due to a relative increase in frictional wall effects. Dividing streamlines also cut relatively deeper into a shallower cavity. Fluid flux into the cavity increases under increasing shear for all cavity geometries and velocity profiles.

Models suggest that shallow cavities with inviscid overlying flow have increased vortex strength as aspect ratio increases up to $AR = 0.5$ (Brandeis, 1982). Wall boundary layers within the pit take up a smaller fraction of the flow in deeper pits, and vortices can spin faster. As aspect ratio further increases ($AR > 0.5$), however, the average velocity within the cavity drops as an increasing amount of low-energy

fluid develops in the cavity bottom, effecting a longer residence time in deeper cavities.

In our three-dimensional pits, the effect of aspect ratio on vortex circulation not only directs fluid residence time, it also determines fluid flux. The rate of vortex spinning affects the cross-stream gradients that force the exit of fluid from the pit. If exit rate of fluid from the pit determines in part the entrance rate of fluid to the pit, then deeper pits should have an increased fluid flux. For near-neutrally buoyant particles, particle flux should approximate fluid flux, and we should expect particle flux to increase with pit aspect ratio. In our experiments, given the same shear velocity and opening diameter, particle flux into the pit increased for $AR = 0.5$ (the critical point observed in two-dimensional systems) and for $AR = 2$, the deepest pit tested. This result refutes the notion that pits of all aspect ratios just receive a “background” downward flux of particles according to their cross-sectional area. The relative increase in vorticity gradients and the intensity of this aspect-ratio effect over the range we tested, however, was much smaller than the effect of flow conditions. Our experiments showed that bed roughness and the turbulence created by a rough bed have a much greater effect on particle flux than pit aspect ratio (compare Figs. 4A and 6A).

Inside the pit, particle flux and residence time are related through particle concentration and pit volume. A typical scaling (Broecker and Peng, 1982) shows that particle residence time (RT) can be approximated by:

$$RT \propto \frac{C_{\text{pit}} V_{\text{pit}}}{C_{\text{flow}} \psi_{\text{flow}} - \psi_{\text{dep}}} = \frac{C_{\text{pit}} V_{\text{pit}}}{\psi_{\text{pit}} - \psi_{\text{dep}}} \quad (1)$$

where C_{pit} is number of particles per volume in the pit, V_{pit} is the volume of the pit, C_{flow} is number of particles per unit of volume outside the pit, ψ_{flow} is the flux of fluid into the pit, ψ_{pit} is the number of beads entering the pit per unit of time, ψ_{dep} is the number of beads depositing to the pit surface per unit of time, and ψ_{dep} is small compared to ψ_{pit} . Fluid residence time decreases with an increased exchange rate of fluid between the pit and the main flow circulation, and thus with the circulation intensity of deeper pits. On the other hand, residence time increases with pit volume and the increase in slowly circulating vortices or “dead space” found in deeper pits. When particles have nearly-neutral buoyancy, particle residence time will scale with fluid residence time. In our experiments, particles showed an increased range of time spent in deeper pits (as illustrated by the greater variance), yet residence time did not vary sharply among most of our treatments (except for the hydraulically rough flow condition). This small range supports the trade-off mentioned above. The effect of the flow field on residence time is of about the same order as that of geometry (compare Figs. 4C and 6C), although opposite in sign.

Absolute residence time does not determine deposition rates directly. We hypothesize that the relationship between residence time and deposition is not linear, but

rather hyperbolic, i.e. deposition increases with increasing residence time to some “saturation point” (or minimum required time) where it then levels off and no longer depends on residence time. The minimum length of time required will depend on the particle settling velocity if deposition is predominantly via gravitational settling. (See Shimeta and Jumars, 1991, for a discussion of particle capture mechanisms.) As long as the residence time is sufficiently long to allow particles to settle through the depth of the pit, increasing it by changes in geometry or flow conditions will not significantly increase deposition. If residence time drops below the necessary level, deposition will decrease, as it did in our hydraulically rough flow treatments (Fig. 7a).

Eq. (1) can be rearranged to predict the resultant pit concentration as a function of excess particle flux, particle residence time, and pit volume:

$$C_{\text{pit}} \propto \frac{RT(\psi_{\text{pit}} - \psi_{\text{dep}})}{V_{\text{pit}}}. \quad (2)$$

Concentration in the pit is directly proportional to particle flux and residence time and inversely proportional to pit volume. In our experiments, the measured decrease in concentration with increasing aspect ratio was due to both residence time and particle flux increasing, while pit volume was increasing by a greater degree. The resultant particle concentration was lower in deeper pits. For a single pit aspect ratio ($AR = 0.5$) under increasingly rough flow, however, the strong increase in particle flux dominates this relationship and greatly increases the concentration of particles in the pit (relative to the source fluid) even though residence time decreases with turbulence.

Further inferences can be drawn from our results and the formulations derived for hydrosol filtration theory (see review by Shimeta and Jumars, 1991, and references therein). Deposition by direct interception should increase with particle diameter, pit surface area, particle flux into the pit, and particle concentration. Under hydraulically smooth flow, interception is restricted near the stagnation line on the downstream side of the pit (see Fig. 2) where streamlines converge and come within one particle diameter of the boundary, or during a particle’s first sweep around the vortex. Under rough flow, when the position of the internal vortex is not fixed, the chances of a particle contacting the pit wall may increase with the number of times it circulates. When wall boundary layers are thinner, during a flow excursion any given streamline could come more easily within a particle diameter of the wall. The rate of deposition by interception should thus increase with increasing aspect ratio and increasing Re_* .

Deposition by inertial impaction depends on the “stopping distance” of the particle ($l_s = (u_* (\rho_p - \rho_f)(2r_p)^2)/18\mu_f$; where r_p is particle radius, and μ_f is dynamic viscosity of the fluid, ν/ρ_f ; Shimeta and Jumars, 1991). With increasing stopping distance, a particle is more likely to encounter the boundary as it diverges from its bending streamline. Thus, deposition by inertial impaction increases with particle

excess density, particle diameter, and fluid velocity, and depends on the path of fluid entering the pit (which is related to pit shape and the position of the dividing streamline). Intensity of inertial impaction should increase with Re_* but is probably not affected much by our experimental range of pit aspect ratios. In our experiments, calculated stopping distances of our particles in the flow range tested are two orders of magnitude smaller than their diameters. Because of their low excess densities, marine flocs probably do not deposit to pits by inertial impaction.

Deposition by gravitational settling depends on particle settling velocity relative to fluid shear velocity (a particle Rouse number), and on the ratio of particle residence time to time required to settle to the bottom. The intensity of gravitational settling should remain nearly constant as long as residence time stays above the critical level, but then decrease with larger Re_* as residence time drops. Since particle flux and concentration also increase with increasing Re_* , however, the rate of deposition by gravity may increase up to the critical residence time, as observed in our experiment. Gravitational settling should show no strong trend with aspect ratio because of the residence time trade-off, except when particle flux and concentration change. Such an effect is difficult to resolve in our experiments because of the coincident increase in particle flux and decrease in concentration observed with increasing aspect ratio.

Pits apparently do not capture particles by centrifugation. Centrifugal acceleration on particles due to their rotation in the vortex ($g_c = r_v \omega^2 \sim 0.25$ to 2.0 cm s^{-2} ; assuming a vortex radius, r_v , of 1 cm and angular velocity, ω , of 0.5 to 1.4 rad s^{-1} , approximated using u_*) is $< 1\%$ of gravitational acceleration ($g \sim 980 \text{ cm s}^{-2}$).

Overall, gravitational settling appears to be the dominant mechanism by which pits capture even low-excess-density particles. In all cases except the hydraulically rough flow condition (when we tested only $AR = 0.5$), sensitivity of deposition rate to residence time was low and the minimum time required for deposition must have been exceeded. Since deposition varied among pit aspect ratios and showed some concentration about attachment lines, however, direct interception may also be operating. The increase in deposition with aspect ratio scales with a coincident increase in pit surface area. Interception may thus become important in deeper pits capturing larger particles. Inertial impaction was probably not a significant mechanism under our experimental conditions since stopping distances were so short and, if important, it would have led to a deposition increase under hydraulically rough flow.

A benthic organism that benefits from localized deposition of low-excess-density particles such as we have modelled, benefits from pit dwelling under nearly all conditions tested here. L. Mayer *et al.* (in review) find flocculent particles to be far higher in labile organic material than are bulk sediments. If gravitational settling is the primary mechanism for capture, then as long as the minimum residence time is achieved by a pit shape in the existing flow field, a deposit feeder need not dig a deeper pit. The utility of digging deeper under smooth flow conditions to increase

surface area and capture even more food will depend on relative rates of deposition and ingestion (Miller *et al.*, 1984).

A deposit feeder might respond to increasing turbulence by digging deeper to maintain the minimum residence time. Deeper pits may work better under hydraulically rough flows than the relatively shallow pit ($AR = 0.5$) examined here. But deeper pits also result in an increased average settling distance for each particle and may hinder deposition if residence time does not increase with depth as fast as the time required for settling. Though we did not test this relationship, field observations support it. The fact that pits are apparently rare in high-energy environments (Yingst and Aller, 1982) may indicate an upper limit to deposition enhancement. Additional experiments comparing deposition and flux to other pit aspect ratios under increasing turbulence must be done to test this possible optimality relationship.

While deposition of particles to the seabed is desirable and necessary for obligate surface and subsurface deposit feeders, it is not required for food capture by suspension feeders. A suspension feeder living on a flat surface would certainly experience a horizontal particle flux in excess of those measured in our pits. If an organism benefits from the reduced velocities of the pit (e.g. for increased retention after contact), it can increase its relative particle flux by digging a deeper pit, or most notably, by living in a shallow pit under rough flow (when a deposit feeder would not benefit). Active suspension feeders with small filtering rates might prefer higher particle concentrations rather than higher fluxes, in which case a shallower pit would work well under any of the flow conditions we tested. This benefit could explain the behavior of ophiuroids that we have observed from *ALVIN* in Santa Catalina Basin, California—resting at the bottom of shallow pits with arms extended presumably to suspension feed. What effect a pit dweller has on the flow pattern and particle behavior within a pit has yet to be explored.

6. Conclusions

Pits could function to improve the diets of deposit-feeding organisms. In our laboratory model that mimicked conditions common to the subtidal and deep-sea benthos, pits captured particles efficiently. Compared to a smooth, flat bed, pits enhanced the deposition rate of particles having large diameter and low excess density by decreasing shear (i.e. lift) on the particles, increasing the particle residence time during which particles can settle from the flow, and increasing the surface area to which a particle can adhere. Deeper pits under hydraulically smooth flow have greater particle fluxes, slightly longer residence times, and greater surface areas, and thus capture more particles than shallow pits. Deposition rate increased to deeper pits because of the greater particle flux arising from stronger cross-stream vorticity gradients. Enhancement due to the increased intensity of interception by deeper pits with greater surface area may also occur. Overall, deposition enhancement by pits is not due entirely to increased surface area, since the degree of

enhancement relative to flat patches exceeds that predicted by a simple increase in surface area. Deposition by gravitational settling probably accounts for this effect and explains the sensitivity of deposition to a sharp decrease in residence time under hydraulically rough flow. The relative importance of these two mechanisms depends on flow field, pit aspect ratio, and particle characteristics. Since overall sensitivity of deposition rate to residence time is low, suggesting that the minimum required time for settling has been exceeded in all but the hydraulically rough flow case, gravitational settling probably dominates pit capture under the conditions that we tested.

Within the range of experimental conditions, a shallow pit ($AR = 0.5$) under hydraulically transitional flow ($Re_* = 60$) captured the most particles per unit of time. A trade-off exists, therefore, between increasing particle flux and decreasing residence time as turbulence increases in the flow overlying shallow pits. Conditions of higher particle concentration and greater particle flux to the pit will not yield deposition if turbulence is so high that the residence time gets too low or high shear near the pit walls prevents particles from depositing. These conditions could benefit pit-dwelling suspension feeders.

Acknowledgments. We would like to thank the Director, A.O.D. Willows, and staff of Friday Harbor Laboratories for use of such fine facilities. We thank B. Dade, J. Deming, E. Flinchem, S. Holland, D. Penry, J. Shimeta, and R. Wheatcroft for valuable contributions to this and earlier drafts. P. Hill analyzed the size-frequency distribution of the latex spheres. We also thank C. A. Butman and an anonymous reviewer for critical comments which greatly strengthened this manuscript. This research was supported by NSF Grant OCE 89-16425.

REFERENCES

- Allredge, A. L. and C. Gotschalk. 1988. *In situ* settling behavior of marine snow. *Limnol. Oceanogr.*, 33, 339–351.
- Aller, J. Y. and R. C. Aller. 1986. Evidence for localized enhancement of biological activity associated with tube and burrow structures in deep-sea sediments at the HEBBLE site, western North Atlantic. *Deep Sea Res.*, 33, 755–790.
- Billheimer, L. E. and B. C. Coull. 1988. Bioturbation and recolonization of meiobenthos in juvenile spot (*Pisces*) feeding pits. *Estuar. Coastal Shelf Sci.*, 27, 335–340.
- Bozeman, J. D. and C. Dalton. 1973. Numerical study of viscous flow in a cavity. *J. Comput. Phys.*, 12, 348–363.
- Brandeis, J. 1982. Flow separation in shear-layer-driven cavities. *AAIAJ.*, 20, 908–914.
- Broecker, W. S. and T.-H. Peng. 1982. *Tracers in the Sea*. Lamont-Doherty Geological Observatory, Palisades, New York, 690 pp.
- Burggraf, O. R. 1966. Analytical and numerical studies of structure of steady separated flows. *J. Fluid Mech.*, 24, 113–151.
- Butman, C. A. 1986. Sediment trap biases in turbulent flows: results from a laboratory flume study. *J. Mar. Res.*, 44, 645–693.
- Butman, C. A., W. D. Grant and K. D. Stolzenbach. 1986. Predictions of sediment trap biases in turbulent flows: a theoretical analysis based on observations from the literature. *J. Mar. Res.*, 44, 601–644.
- Cook, D. O. 1971. Depressions in shallow marine sediment made by benthic fish. *J. Sed. Petr.*, 41, 577–578.

- Eckman, J. E., A. R. M. Nowell and P. A. Jumars. 1981. Sediment destabilizations by animal tubes. *J. Mar. Res.*, *39*, 361–374.
- Gardner, W. D. 1980a. Sediment trap dynamics and calibration: a laboratory evaluation. *J. Mar. Res.*, *38*, 17–39.
- 1980b. Field assessment of sediment traps. *J. Mar. Res.*, *38*, 41–52.
- Greenspan, D. 1969. Numerical studies of prototype cavity flow problems. *Comp. J.*, *12*, 88–93.
- Gross, T. F. and W. B. Dade. 1991. Suspended sediment storm modeling. *Mar. Geol.*, *99*, 343–360.
- Hannan, C. A. 1984. Initial settlement of marine invertebrate larvae: The role of passive sinking in a near-bottom turbulent flow environment. Doctoral dissertation, W.H.O.I./M.I.T. Joint Program, 534 pp.
- Heezen, B. C. and C. D. Hollister. 1971. *The Face of the Deep*. Oxford University Press, New York, 659 pp.
- Hollander, M. and D. A. Wolfe. 1973. *Nonparametric Statistical Methods*. John Wiley & Sons, New York, 503 pp.
- Howard, J. D. and J. Dörjes. 1972. Animal-sediment relationships in two beach-related tidal flats; Sapelo Island, Georgia. *J. Sed. Petr.*, *42*, 608–623.
- Howard, J. D., T. V. Mayou and R. W. Heard. 1977. Biogenic sedimentary structures formed by rays. *J. Sed. Petr.*, *47*, 339–346.
- Isaacson, E. de St. Q. and M. de St. Q. Isaacson. 1975. *Dimensional Methods in Engineering and Physics*. Wiley, New York, 220 pp.
- Jumars, P. A., L. M. Mayer, J. W. Deming, J. A. Baross and R. W. Wheatcroft. 1990. Deep-sea deposit-feeding strategies suggested by environmental and feeding constraints. *Phil. Trans. R. Soc. Lond. A*, *331*, 85–101.
- Kawaguti, M. 1961. Numerical solutions of the Navier-Stokes equations for the flow in a two-dimensional cavity. *J. Phys. Soc. Jpn.*, *16*, 2307–2318.
- Mauviel, A., S. K. Juniper and M. Sibuet. 1987. Discovery of an enteropneust associated with a mound-burrow trace in the deep sea: ecological and geochemical implications. *Deep-Sea Res.*, *34*, 329–335.
- McCave, I.N. 1984a. Size-spectra and aggregation of suspended particles in the deep ocean. *Deep Sea Res.*, *31*, 329–352.
- 1984b. Erosion, transport and deposition of fine-grained marine sediments, *in* *Fine-grained Sediments: Deep Sea Processes and Facies*, D. A. V. Stow and D. J. W. Piper, eds., Special Publication 15, Geol. Soc. of London, 35–69.
- Middleton, G. V. and J. B. Southard. 1985. *Mechanics of Sediment Movement*, 2nd ed., Short course 3, Soc. Econ. Paleon. Min., Tulsa, OK, 401 pp.
- Miller, D. C. 1989. Abrasion effects on microbes. *Mar. Ecol. Prog. Ser.*, *55*, 73–82.
- Miller, D. C., P. A. Jumars and A. R. M. Nowell. 1984. Effects of sediment transport on deposit feeding: scaling arguments. *Limnol. Oceanogr.*, *29*, 1202–1217.
- Mills, R. D. 1965a. On the closed motion of a fluid in a square cavity. *J. Roy. Aero. Soc.*, *69*, 116–120.
- 1965b. Numerical solutions of viscous flow equations for a class of closed flows. *J. Roy. Aero. Soc.*, *69*, 714–718.
- Moffatt, H. K. 1964. Viscous and resistive eddies near a sharp corner. *J. Fluid Mech.*, *18*, 1–18.
- Myers, A. C. 1977a. Sediment processing in a marine subtidal sandy bottom community. 1. Physical aspects. *J. Mar. Res.*, *35*, 609–632.
- 1977b. Sediment processing in a marine subtidal sandy bottom community. 2. Biological consequences. *J. Mar. Res.*, *35*, 633–647.

- Nallasamy, M., and K. K. Prasad. 1977. Cavity flow at high Reynolds-numbers. *J. Fluid Mech.*, 79, 391–414.
- Nelson, C. H., K. R. Johnson and J. H. Barber. 1987. Gray whale and walrus feeding excavation on the Bering Shelf, Alaska. *J. Sed. Petr.*, 57, 419–430.
- Nowell, A. R. M. and P. A. Jumars. 1984. Flow environments of aquatic benthos. *Ann. Rev. Ecol. Syst.*, 15, 303–328.
- . 1987. Flumes: Theoretical and experimental considerations for simulation of benthic environments. *Oceanogr. Mar. Biol. Ann. Rev.*, 25, 91–112.
- Nowell, A. R. M., P. A. Jumars and K. Fauchald. 1984. The foraging strategy of a subtidal and deep-sea deposit feeder. *Limnol. Oceanogr.*, 29, 645–649.
- O'Brien, V. 1972. Closed streamlines associated with channel flow over a cavity. *Phys. Fluids*, 15, 2089–2097.
- Palmer, M. 1988. Epibenthic predators and marine meiofauna: separating predation, disturbance, and hydrodynamic effects. *Ecology*, 69, 1251–1259.
- Pan, F. and A. Acrivos. 1967. Steady flows in rectangular cavities. *J. Fluid Mech.*, 28, 643–655.
- Pemberton, S. G., R. W. Frey and R. G. Bromley. 1988. The ichnotaxonomy of *Conostichus* and other plug-shaped ichnofossils. *Can. J. Earth Sci.*, 25, 866–892.
- Ratkowsky, D. A. and Z. Rotem. 1968. Viscous flow in a rectangular cut out. *Phys. Fluids*, 11, 2761–2763.
- Risk, M. J. and H. D. Craig. 1976. Flatfish feeding traces in Minas Basin. *J. Sed. Petr.*, 467, 411–413.
- Self, R. F. L., A. R. M. Nowell and P. A. Jumars. 1989. Factors controlling critical shears for deposition and erosion of individual grains. *Mar. Geol.*, 86, 181–199.
- Shimeta, J. and P. A. Jumars. 1991. Physical mechanisms and rates of particle capture by suspension-feeders. *Oceanogr. Mar. Biol. Ecol. Ann. Rev.*, 29, 191–257.
- Sinha, S. N., A. K. Gupta and M. M. Oberai. 1982. Laminar separating over backsteps and cavities. 2. Cavities. *AAIAJ.*, 20, 370–375.
- Smith, D. L. O. and R. A. Lohnes. 1984. Behavior of bulk solids, in *Particle Characterization in Technology*, Vol. 1, J. K. Beddow, ed., CRC Press, Boca Raton, Florida, 101–133.
- Sokal, R. R. and F. J. Rohlf. 1981. *Biometry: The Principles and Practice of Statistics in Biological Research*. W. H. Freeman and Company, San Francisco, 859 pp.
- Soluk, D. A. and D. A. Craig. 1988. Vortex feeding from pits in the sand: a unique method of suspension feeding used by a stream invertebrate. *Limnol. Oceanogr.*, 33, 638–645.
- Stephens, D. W. and J. R. Krebs. 1986. *Foraging Theory; Monographs in Behavioral Ecology*. Princeton University Press, Princeton, New Jersey, 256 p.
- Taghon, G. L. 1988. The benefits and costs of deposit feeding in the polychaete *Abarenicola pacifica*. *Limnol. Oceanogr.* 33, 1166–1175.
- Taghon, G. L., A. R. M. Nowell and P. A. Jumars. 1984. Transport and breakdown of fecal pellets: biological and sedimentological consequences. *Limnol. Oceanogr.*, 29, 64–72.
- Takematsu, M. 1965. Viscous flow in a two-dimensional cavity. *J. Phys. Soc. Jpn.*, 20, 283.
- . 1966. Slow viscous flow past a cavity. *J. Phys. Soc. Jpn.*, 21, 1816–1821.
- Taneda, S. 1979. Visualizations of separating Stokes flows. *J. Phys. Soc. Jpn.*, 46, 1935–1942.
- Theil, H., O. Pfannkuche, G. Shriver, K. Lochte, A. J. Gooday, C. Hembleben, R. F. C. Mantoura, C. M. Turley, J. W. Patching and F. Riemann. 1988. Phytodetritus on the deep-sea floor in a central oceanic region of the Northeast Atlantic. *Biol. Oceanogr.*, 6, 203–239.
- Thistle, D. 1981. Natural physical disturbances and communities of marine soft bottoms. *Mar. Ecol. Progr. Ser.*, 6, 223–228.

- Torrance, K. and H. Zien. 1972. Cavity flows driven by buoyancy and shear. *J. Fluid Mech.*, 51, 221–231.
- VanBlaricom, G. R. 1982. Experimental analyses of structural regulation in a marine sand community exposed to oceanic swell. *Ecol. Monogr.*, 52, 283–305.
- Weiss, R. F. and B. H. Florsheim. 1965. Flow in a cavity at low Reynolds number. *Phys. Fluids*, 8, 1631–1635.
- Wheatcroft, R. A. 1990. Rates and Pathways of Sediment Bioturbation: A Mechanistic Approach. Doctoral dissertation, Univ. of Washington, 197 pp.
- Yingst, J. Y. and R. C. Aller. 1982. Biological activity and associated sedimentary structures in HEBBLE-area deposits, western North Atlantic. *Mar. Geol.*, 48, M7-M15.